THE JOURNAL OF PHYSICAL CHEMISTRY B

Article

pubs.acs.org/JPCB

Dispersion of Linear, Nonlinear Optical Susceptibilities and Hyperpolarizability of $C_{11}H_8N_2O$ (*o*-Methoxydicyanovinylbenzene) Crystals

Ali H. Reshak,*[,†,‡] H. Kamarudin,[‡] I. V. Kityk,[§,⊥] and S. Auluck[∥]

[†]School of Complex systems, FFPW, CENAKVA, University of South Bohemia in CB, Nove Hrady 37333, Czech Republic
[‡]School of Material Engineering, Malaysia University of Perlis, P.O. Box 77, d/a Pejabat Pos Besar, 01007 Kangar, Perlis, Malaysia
[§]Electrical Engineering Department, Technological University of Czestochowa, Al.Armii Krajowej 17/19, Czestochowa, Poland
[∥]Council of Scientific and Industrial Research - National Physical Laboratory Dr. K S Krishnan Marg, New Delhi 110012, India
[⊥]Eastern European National University, pr. Voli 13, UA-43025, Lutsk, Ukraine

ABSTRACT: Linear and nonlinear optical susceptibility dispersion and hyperpolarizability of $C_{11}H_8N_2O$, *o*-methoxydicyanovinylbenzene, crystals were performed by means of density functional theory (DFT). The exchange and correlation potential was described within a framework of the local density approximation (CA-LDA) and gradient approximation (GGA) based on exchange-correlation energy optimization to calculate the total energy. Engel-Vosko generalized gradient approximation (EV-GGA) and the modified Becke-Johnson potential (mBJ) were used for the electronic crystal structure and optical susceptibility dispersion calculations. We have established systematically increasing energy gap from 2.25 eV (LDA), 2.34 eV (GGA), 2.50 eV (EVGGA), and 2.96 eV (mBJ). The crystal possesses a direct band gap which is an important key factor to make the crystal optically active with high linear and nonlinear optical susceptibilities and hyperpolarizability. Additionally, the studied crystal has a considerable anisotropy of birefringence which is necessary for phase matching conditions during the optical second harmonic experiments. We have found that the theoretically evaluated second harmonic generation achieves about 5.8×10^{-8} esu in good agreement with the experimental value (4.9×10^{-8} esu). Additionally, we have found that our calculated value of β_{222} is about 2.3×10^{-30} esu at zero energy and 6.6×10^{-30} esu at $\lambda = 1.064$ μm. We should emphasize that our calculated value of β_{222} (6.60×10^{-30} esu at $\lambda = 1.064$ μm) shows better agreement with the experimental data (5.04×10^{-30} esu at $\lambda = 1.064$ μm) than other calculations.

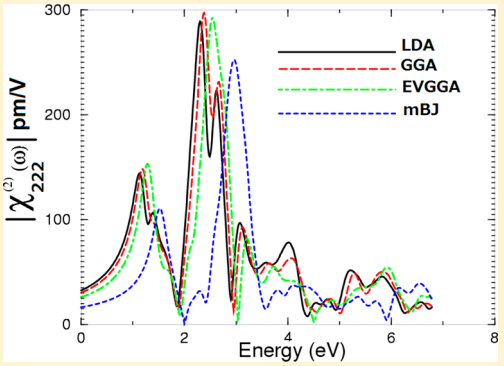

1. INTRODUCTION

Structural studies of polarized organic molecules as components for nonlinear optical (NLO) and photorefractive materials are a subject of intense scientific and technological studies and have attracted a great deal of attention in the past two decades.[1] They have crucial advantages in comparison with currently used inorganic crystals due to their ultrafast response time and low dielectric constants.[1] NLO properties of organic molecules are the subject of very intensive studies in recent years because of their potential applicability for electro-optical modulation, frequency mixing, second harmonic generation (SHG), and fabrication of many optical devices.[2,3] To possess NLO properties, organic molecules should contain a polar and highly π-conjugated electron system terminated with electron donor and acceptor groups. One such compound is the titled compound which crystallizes in a non-centrosymmetric space group to allows SHG. Functionalized aromatic groups with both π-electron-donating and π-electron-accepting groups, such as the classical NLO chromophore 2-methlyl-4-nitroaniline,[4] are among the typical organic NLO materials. The establishment of molecular asymmetry or chirality is a promising strategy to achieve centrosymmetric or non-centrosymmetric packing. The supramolecular packing will be governed by steric interactions and van der Waals forces. Usually in crystal structure, the molecules are linked by noncovalent intermolecular interactions such as electrostatic interactions, van der Waals interactions, and hydrogen bonds.[5,6] During crystal growth, the molecules tend to undergo shape simplification, which gives rise to dimers and then to high-order aggregates in order to adapt to a close-packing in the solid state. The high tendency of achiral molecules to crystallize centrosymmetrically could be due to such a close-packing driving force. Therefore, if the symmetry of the chromophores is reduced, dimerization and subsequent aggregation is no longer an advantage to the close packing and increases the probability of acentric crystallization. The symmetry reduction can be achieved either by incorporation of steric substituents into the chromophore or introduction of molecular asymmetry. Also, the hydrogen bond functionalities may be included to promote a desired chromophore packing. The Coulomb intermolecular forces are used to charge the chromophores in combination with counterions that tend to override

Received: July 26, 2012
Revised: October 18, 2012
Published: October 23, 2012

the weaker dipole−dipole interactions and promote a noncentrosymmetric packing which is required for second-order nonlinear optical susceptibilities.[7] For the organic NLO crystals, it is well-known that a different orientation of chromophores essentially affects the macroscopic NLO susceptibilities.[8,9]

In recent years, density functional theory (DFT) becomes an increasingly useful tool to intrepet experimental studies. The success of DFT is mainly due to the fact that it describes small molecules more reliably than Hartree−Fock theory. It is also computationally more economical than wave function based methods with inclusion of electron correlations.[10,11] Using the DFT to study the relationship between structure and the optical susceptibilities may sometimes be a better solution before venturing into the physical growth of the crystals. The DFT calculations have been extensively used for the computations of structural and optical parameters to explore the relationship between them. The present study is an attempt to understand an interesting NLO organic system. The current calculations are based on one of the accurate methods for computation of the electronic structure of solids within a framework of DFT.[12,13] It is called the all-electron full potential linear augmented plane wave (FP-LAPW) method. Such a study is all the more interesting, as the structure of this compound has been determined by Antipin et al.[14] using X-ray diffraction. Beyond this, not much is known about this compound. We hope that our study will be a step in this direction.

In the next section, we briefly describe the calculation procedure and give the computational details. In section 3, we report and discuss our result. Finally, conclusions will be given in section 4.

2. STRUCTURAL PROPERTIES AND COMPUTATIONAL DETAILS

Acentric monoclinic $C_{11}H_8N_2O$, *o*-methoxydicyanovinylbenzene, also called DIVA crystals, possesses *P*21 space group with unit cell dimensions $a = 7.922(2)$ Å, $b = 5.402(2)$ Å, $c = 11.375(2)$ Å, and $\beta = 93.58(2)°$. Figure 1 shows the single molecules of

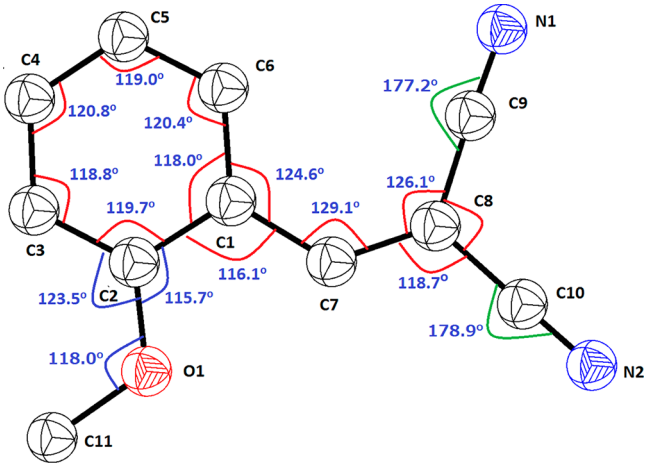

Figure 1. Single molecules along with the calculated bond angles (°).

o-methoxydicyanovinylbenzene (DIVA) along with the calculated bond angles. It was found that the molecular dipole moment orientation with respect to the polar crystal axis is close to the "optimal" value, which is important for the high NLO responses.[14] We have optimized the X-ray crystallographic of DIVA (see Table 1) by minimization of the forces (1 mRy/au) acting on the atoms, using the general gradient Perdew-Burke-Ernzerhof (GGA-PBE)[18] exchange correlation potential keeping, the lattice parameters fixed at the experimental values. The electronic structure and linear and nonlinear optical susceptibilities were determined from the relaxed geometry. The self-consistent density at these positions can be found after the forces are minimized by turning off the relaxations and driving the system to achieve self-consistency. The all-electron full potential linearized augmented plane wave (FP-LAPW) method[15] is employed. This is an implementation of the DFT[16] with different possible approximation for the exchange correlation (xc) potentials. Exchange and correlation potential was described by the local density approximation (CA-LDA)[17] and gradient approximation (GGA),[18] which is based on exchange-correlation energy optimization to calculate the total energy. To overcome the underestimation of the energy gap by LDA and GGA, we have used Engel-Vosko generalized gradient approximation (EV-GGA)[19] and the modified Becke-Johnson potential (mBJ),[20] which optimizes the corresponding potential for electronic band structure and linear and nonlinear optical susceptibility calculations. Our calculations will demonstrate the effect of the four different kinds of exchange-correlation potentials on the linear and nonlinear optical susceptibilities. In order to get the total energy convergence, the basis functions in the interstitial regions (IR) were expanded up to $R_{mt} \times K_{max} = 7.0$ and inside the atomic spheres is the wave function. The maximum value of $\boldsymbol{l}$ were taken as $\boldsymbol{l}_{max} = 10$, while the charge density is Fourier expanded up to $G_{max} = 20$ (a.u.)$^{-1}$. We have used 35 **k**-points in the irreducible Brillouin zone (IBZ) for structural optimization. For the calculation of electronic properties, 180 **k**-points within the BZ and 1000 **k**-points for the calculation of the linear and nonlinear optical susceptibilities were used.

3. RESULTS AND DISCUSSION

3.1. Linear Optical Susceptibilities. Further insight into the electronic structure of the titled compound can be obtained from the calculation of interband optical functions, by summing the transitions from occupied to unoccupied states over whole BZ points. The titled compound crystallizes in monoclinic space groups so there are many nonzero components of the dielectric tensor. We will concentrate on the major components $\varepsilon^{xx}(\omega)$, $\varepsilon^{yy}(\omega)$, and $\varepsilon^{zz}(\omega)$ corresponding to electric field vector polarized along the crystallographic axes **a**, **b**, and **c**.

The imaginary parts $\varepsilon_2^{xx}(\omega)$, $\varepsilon_2^{yy}(\omega)$, and $\varepsilon_2^{zz}(\omega)$ for the three principal complex tensors are calculated. The half-width broadening due to electron−phonon interaction is taken to be 0.1 eV, which is typical of the experimental accuracy. We have calculated the dispersions for the imaginary part of the linear optical response using LDA, GGA, EVGGA, and mBJ approaches. In Figure 2a, we have plotted the $\varepsilon_2^{average}(\omega)$ of $\varepsilon_2^{xx}(\omega)$, $\varepsilon_2^{yy}(\omega)$, and $\varepsilon_2^{zz}(\omega)$ for each xc individually in order to seek the influence of each xc on the linear optical response. Following this figure, we can establish that whole linear optical spectra shift toward higher energies as we go from LDA to GGA, EVGGA, and mBJ. The spectral peaks in the optical response are caused by the electric dipole transitions between the valence and conduction bands. Our analysis of optical response features shows that the edges of optical absorption are situated at 2.25 eV (LDA), 2.34 eV (GGA), 2.50 eV (EVGGA), and 2.96 eV (mBJ). These points can be assigned to $Z_v - Z_c$ band energy splitting which gives the minimal thresholds for optical transitions between VBM and CBM. We should emphasizes that mBJ brings the optical gap close to the experimental value. For this reason, in Figure 2b we

dx.doi.org/10.1021/jp3074128 | J. Phys. Chem. B 2012, 116, 13338−13343

Table 1. Calculated Atomic Positions (Optimized) in Comparison with the Experimental Ones[14]

atom	*x*-exp (XRD)	*x*-calcd (optimized)	*y*-exp (XRD)	*y*-calcd (optimized)	*z*-exp (XRD)	*z*-calcd (optimized)
O (1)	0.0070 (2)	0.01133043	0.6600 (5)	0.63464119	0.1545 (1)	0.03731566
N (1)	0.5923 (2)	0.61489008	0.7966 (5)	0.83887628	0.3093 (1)	0.30337712
N (2)	0.3624 (2)	0.38371504	0.2834 (4)	0.32607832	0.0339 (1)	0.03613963
C (1)	0.9276 (2)	0.95987416	0.3251 (4)	0.36544200	0.2667 (1)	0.26592959
C (2)	0.0536 (2)	0.10080640	0.4972 (5)	0.51490776	0.2434 (1)	0.24320587
C (3)	0.2148 (2)	0.25789842	0.4924 (5)	0.48365924	0.3100 (1)	0.31390031
C (4)	0.2501 (2)	0.27912348	0.3199 (5)	0.31568550	0.3993 (1)	0.40771115
C (5)	0.1281 (2)	0.14072354	0.1503 (4)	0.17369404	0.4247 (1)	0.43284252
C (6)	0.9681 (2)	0.98430736	0.1532 (4)	0.19746182	0.3586 (1)	0.36238711
C (7)	0.7647 (2)	0.79713160	0.3407 (4)	0.38920585	0.1919 (1)	0.19141838
C (8)	0.6273 (2)	0.65581606	0.1887 (4)	0.238923023	0.1857 (1)	0.18416203
C (9)	0.6111 (2)	0.63727134	0.9705 (4)	0.01953659	0.2553 (1)	0.25101752
C (10)	0.4794 (2)	0.50793546	0.2432 (4)	0.29184186	0.1012 (1)	0.10164968
C (11)	0.1323 (2)	0.09192992	0.8282 (5)	0.71585218	0.1217 (1)	0.15043163
H (1)	0.3033 (29)	0.36627702	0.6079 (52)	0.59547134	0.2992 (21)	0.29496257
H (2)	0.3660 (34)	0.40289242	0.2910 (54)	0.29652063	0.4405 (22)	0.46218899
H (3)	0.1537 (31)	0.15472506	0.0256 (69)	0.04529797	0.4786 (24)	0.50770194
H (4)	0.8855 (28)	0.87767842	0.0457 (52)	0.08615525	0.3767 (19)	0.38395006
H (5)	0.7478 (25)	0.78512865	0.4694 (51)	0.54351211	0.1396 (18)	0.12859405
H (6)	0.1755 (30)	0.02157593	0.9204 (63)	0.87625434	0.1962 (24)	0.18053716
H (7)	0.2305 (34)	0.22317082	0.7371 (63)	0.78040344	0.0934 (23)	0.14434936
H (8)	0.0759 (27)	0.97419803	0.9350 (55)	0.78777350	0.0586 (19)	0.99449363

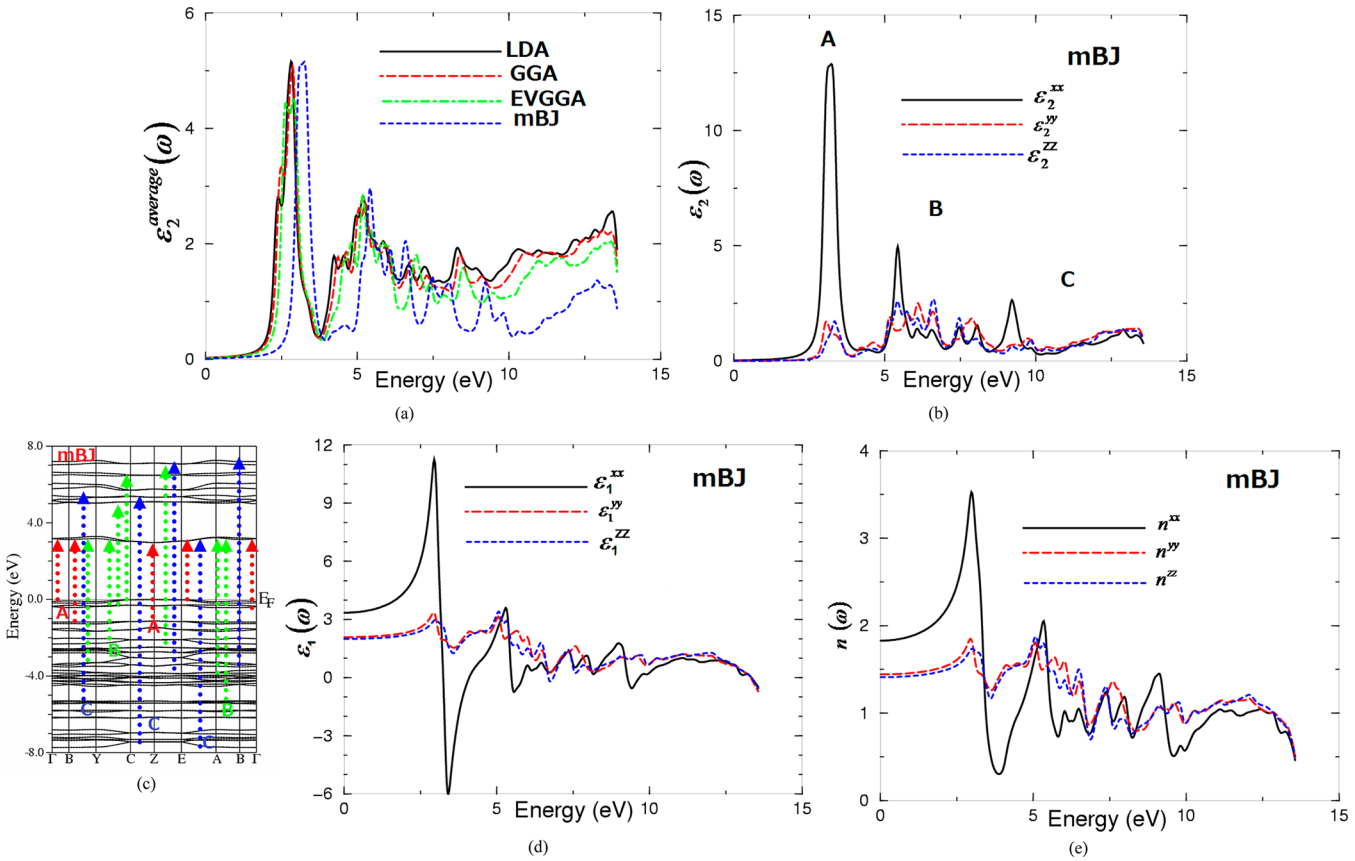

Figure 2. (a) Calculated $\varepsilon_2^{average}(\omega)$ using LDA, GGA, EVGGA, and mBJ. (b) Calculated $\varepsilon_2^{xx}(\omega)$ (black solid curve), $\varepsilon_2^{yy}(\omega)$ (red dashed curve), and $\varepsilon_2^{zz}(\omega)$ (blue dotted dashed curve) dispersion spectra using mBJ. (c) Optical transitions depicted on a generic band structure. (d) Calculated $\varepsilon_1^{xx}(\omega)$ (black solid curve), $\varepsilon_1^{yy}(\omega)$ (red dashed curve), and $\varepsilon_1^{zz}(\omega)$ (blue dotted dashed curve) spectra using mBJ. (e) Calculated $n^{xx}(\omega)$ (black solid curve), $n^{yy}(\omega)$ (red dashed curve), and $n^{zz}(\omega)$ (blue dotted dashed curve) spectra using mBJ.

show $\varepsilon_2^{xx}(\omega)$, $\varepsilon_2^{yy}(\omega)$, and $\varepsilon_2^{zz}(\omega)$ for mBJ. These components are very anisotropic especially at around 3.0 eV. There are three principal spectral structures (A, B, C) in the linear optical spectra. The weakness of the structures B and C compared to A could be explained by the fact that $\varepsilon_2(\omega)$ scales as $1/\omega^2$. To identify these main structures (A, B, C), we should consider the magnitude of

dx.doi.org/10.1021/jp3074128 | J. Phys. Chem. B 2012, 116, 13338−13343

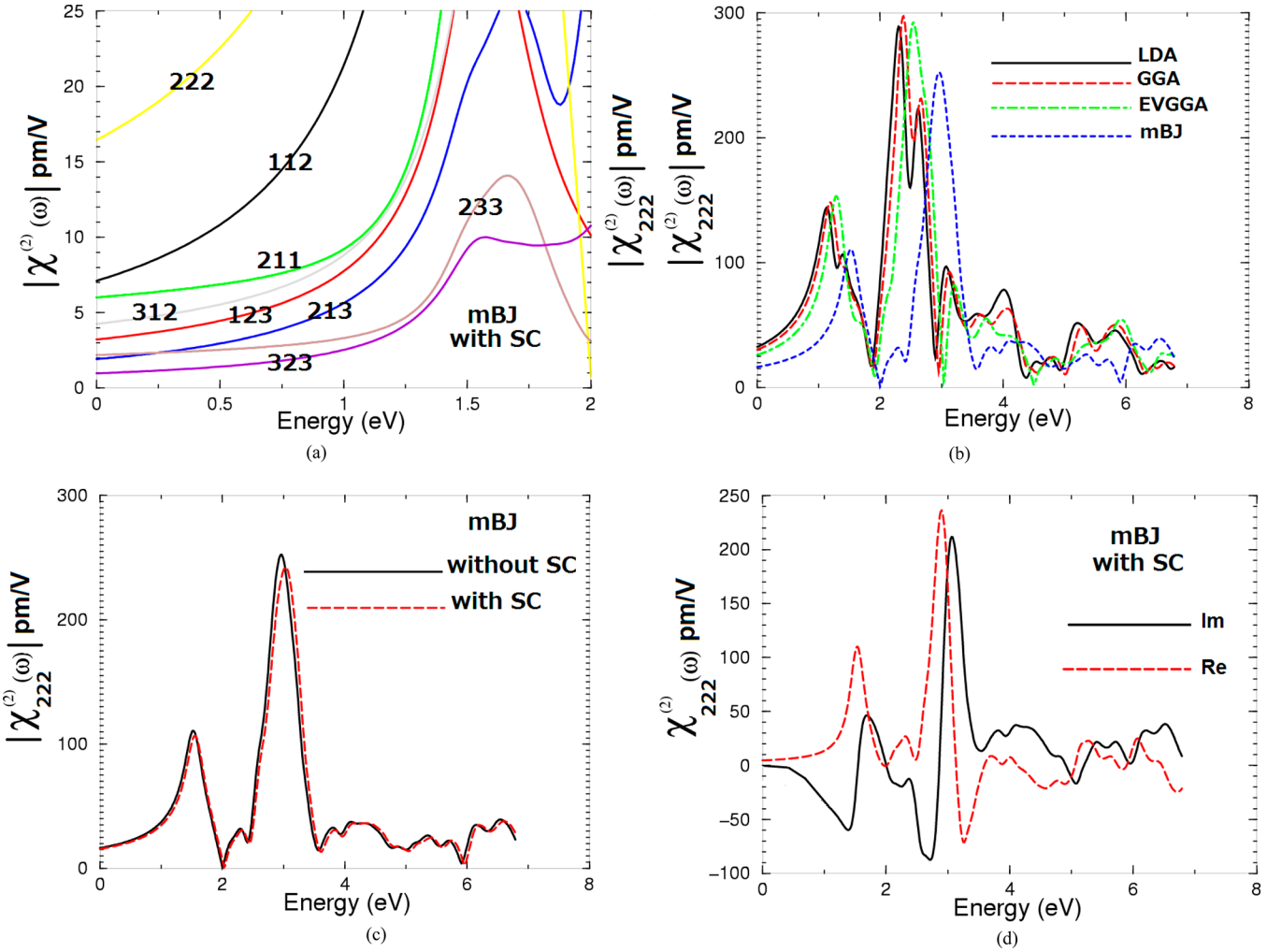

Figure 3. (a) Calculated$|\chi^{(2)}_{ijk}(\omega)|$ for the eight components using mBJ with scissors correction. (b) Calculated $|\chi^{(2)}_{222}(\omega)|$ the dominant component using LDA, GGA, EVGGA, and mBJ with scissors correction. (c) Calculated imaginary $\chi^{(2)}_{222}(\omega)$ (black solid curve) and real $\chi^{(2)}_{222}(\omega)$ (red dashed curve) spectra, using EVGGA with scissors correction.

the optical transition dipole matrix elements. The observed structures should correspond to those transitions which have larger optical matrix dipole transition matrix elements. Since the optical spectra are obtained from the interband transition, it would be worthwhile to attempt to identify the interband transitions that are responsible for the spectral features in $\varepsilon_2^{xx}(\omega)$, $\varepsilon_2^{yy}(\omega)$, and $\varepsilon_2^{zz}(\omega)$ using our calculated band structure and density of states. Figure 2c shows the transitions which are responsible for the principal spectral structures in $\varepsilon_2^{xx}(\omega)$, $\varepsilon_2^{yy}(\omega)$, and $\varepsilon_2^{zz}(\omega)$ dispersions. For convenience, we have labeled the transitions in Figure 2c as A, B, and C. The transitions A are responsible for the structures in $\varepsilon_2^{xx}(\omega)$, $\varepsilon_2^{yy}(\omega)$, and $\varepsilon_2^{zz}(\omega)$ for energies up to 5.0 eV, transitions B for the structures in the energy range 5.0−10.0 eV, and transitions C for the structures between 10.0 and 14.0 eV. The real parts, shown in Figure 2d, are obtained using Kramers−Kronig relations.[21] It is clear that there exists considerable anisotropy at energies lower than 5.0 eV. The static dielectric constants $\varepsilon_1^{xx}(0)$, $\varepsilon_1^{yy}(0)$, and $\varepsilon_1^{zz}(0)$ are listed in Table 2. Note that we do not include phonon contributions to the dielectric screening.

Using the calculated imaginary and real parts of the dielectric function's dispersions, we have evaluated refractive indices and hence the birefringence. Following the refractivity spectra, shown in Figure 2e, we can see again that there is a considerable

Table 2. Calculated $\varepsilon_1^{xx}(0)$, $\varepsilon_1^{yy}(0)$, $\varepsilon_1^{zz}(0)$, $n^{xx}(\omega)$, $n^{yy}(\omega)$, $n^{zz}(\omega)$, and $\Delta n(\omega)$

	theoretical
$\varepsilon_1^{xx}(\omega)$	$\varepsilon_1^{xx}(0)$ = 3.35
	$\varepsilon_1^{xx}(\omega)$ at (1064 nm) = 3.63
$\varepsilon_1^{yy}(\omega)$	$\varepsilon_1^{yy}(0)$ = 2.09
	$\varepsilon_1^{yy}(\omega)$ at (1064 nm) = 2.15
$\varepsilon_1^{zz}(\omega)$	$\varepsilon_1^{zz}(0)$ = 1.99
	$\varepsilon_1^{zz}(\omega)$ at (1064 nm) = 2.05
$n^{xx}(\omega)$	$n^{xx}(0)$ = 1.83
	$n^{xx}(\omega)$at (1064 nm) = 1.91
$n^{yy}(\omega)$	$n^{yy}(0)$ = 1.45
	$n^{yy}(\omega)$at (1064 nm) = 1.47
$n^{zz}(\omega)$	$n^{zz}(0)$ = 1.41
	$n^{zz}(\omega)$at (1064 nm) = 1.43
$\Delta n(\omega)$	$\Delta n(0)$ = 0.40
	$\Delta n(\omega)$ at (1064 nm) = 0.46

anisotropy. We should emphasize that the anisotropy in the linear optical susceptibilities favors enhanced phase matching conditions necessary for observation of the SHG and optical parametric oscillation (OPO). The birefringence $\Delta n(\omega) = n_e(\omega) - n_o(\omega)$ can

dx.doi.org/10.1021/jp3074128 | J. Phys. Chem. B 2012, 116, 13338−13343

Table 3. Calculated $|\chi^{(2)}_{ijk}(0)|$ and $|\chi^{(2)}_{ijk}(\omega)|$ in pm/V at λ = 1064 nm along with d_{ijk} Values[a]

tensor components	theory $\chi^{(2)}_{ijk}(0)$ in (pm/V)	theory $d_{ijk} = 0.5\chi^{(2)}_{ijk}(0)$ in (pm/V)	theory $\chi^{(2)}_{ijk}(\omega)$ in (pm/V) at λ=1064 nm	theory $d_{ijk} = 0.5\chi^{(2)}_{ijk}(\omega)$ in (pm/V) at λ=1064 nm	exp
$\|\chi^{(2)}_{112}(\omega)\|$	7.0	3.5	30.5	15.3	
$\|\chi^{(2)}_{123}(\omega)\|$	3.2	1.6	10.5	5.3	
$\|\chi^{(2)}_{211}(\omega)\|$	6.0	3.0	12.0	6.0	
$\|\chi^{(2)}_{213}(\omega)\|$	2.0	1.0	7.6	3.8	
$\|\chi^{(2)}_{222}(\omega)\|$	16.8	8.4	49.0	24.5 = 5.8×10^{-8} esu	4.9×10^{-8} esu[b]
$\|\chi^{(2)}_{233}(\omega)\|$	2.2	1.1	4.0	2.0	
$\|\chi^{(2)}_{312}(\omega)\|$	4.3	2.2	11.5	5.8	
$\|\chi^{(2)}_{323}(\omega)\|$	1.0	0.5	3.5	1.8	

[a]Where 1 pm/V = 2.387×10^{-9} esu. The calculated values in this table are done using mBJ. [b]Ref 14.

be evaluated from the linear response functions from which the anisotropy of the ordinary $n_o(\omega)$ and extraordinary $n_e(\omega)$ refractive indices is determined. It is clear that the birefringence is crucial only in the nonabsorbing spectral range, which is below the energy gap. The value of the birefringence and the corresponding refractive indices at the static limit and at λ = 1.064 μm are presented in Table 2.

3.2. Nonlinear Optical Susceptibilities and Hyperpolarizability. The origin of nonlinear optical susceptibility dispersions is substantially complicated with respect to linear ones. The difficulties concern not only physical origin, but also the numerical technology. It is caused by the fact that more **k**-points are required to reach a reasonable accuracy. Usually, the second-order nonlinear optical susceptibility is more sensitive to small changes in the band structure than the linear optical properties. Hence, any anisotropy in the linear optical property dispersion is enhanced in the nonlinear spectra. This is a consequence of a fact that the second harmonic response $\chi^{(2)}_{ijk}(\omega)$ involves both the 2ω resonances as well as traditional linear ω resonances. Furthermore, both ω and 2ω resonances can be separated into interband and intraband contributions. The titled non-centrosymmetric compound with monoclinic symmetry possess eight independent nonzero tensor components: $\chi^{(2)}_{112}(\omega)$, $\chi^{(2)}_{123}(\omega)$, $\chi^{(2)}_{211}(\omega)$, $\chi^{(2)}_{213}(\omega)$, $\chi^{(2)}_{222}(\omega)$, $\chi^{(2)}_{233}(\omega)$, $\chi^{(2)}_{312}(\omega)$, and $\chi^{(2)}_{323}(\omega)$. We have calculated the imaginary, real parts, the absolute values, and the static limits for the eight components. From Figure.3a, one can see that $\chi^{(2)}_{222}(\omega)$ is the dominant component which possesses the highest value of SHG.

The well-known LDA and GGA underestimation of the energy band gaps may lead to incorrect values of second-order nonlinear optical susceptibility tensor components, since they are more sensitive to the band gaps with respect to linear-response values due to higher power energy differences in the denominators of the formulas of complex second-order nonlinear optical susceptibility tensors presented in refs 22−24. To overcome the underestimation of LDA, GGA, and EVGGA approaches, we have used mBJ (see Figure 3b). From our experiences with mBJ,[25,20] we assume that the mBJ underestimates the energy gap by around 2%. Hence, we estimate the experimental gap to be 3.026 eV. Then, we introduce quasi-particle self-energy corrections at the level of scissors operators in which the energy bands are rigidly shifted to merely bringing the calculated energy gap closer to the experimental gap value (see Figure 3c). The second-order nonlinear optical susceptibility is very sensitive to the scissors correction. In our previous work using LDA, GGA, and EVGGA, we have found that the scissors correction has a significant effect on the magnitude of $\chi^{(2)}_{ijk}(\omega)$,[26,27] but with the aid of mBJ, the calculated value of the energy gap improved and correspondingly the scissors correction has marginal influence (see Figure 3c). The calculated dispersions of imaginary and real parts of complex second-order nonlinear optical susceptibility tensors for the $\chi^{(2)}_{222}(\omega)$ component are shown in Figure 3d. The calculated values of the second-order susceptibility tensor components at static limits $|\chi^{(2)}_{ijk}(0)|$ and $|\chi^{(2)}_{ijk}(\omega)|$ at λ = 1.064 μm (1.165 eV) are listed in Table 3. We have found that the dominant component of the SHG have a value of about 5.8×10^{-8} esu, which is in good agreement with the measured value (4.9×10^{-8} esu). The static values of the second-order susceptibility tensor are very important and can be used to estimate the output SHG efficiency.

We have calculated the microscopic hyperpolarizability, β_{222}, in particular, the vector components along the dipole moment direction with respect to crystal axes, using the expression give in refs 28,29 $\beta_{ijk} = \chi^{(2)}_{ijk}/Nf^3$, where ($N$) is the number of molecules/cm^3 and (f) is the local field factor, the value of (f) is varying between 1.3 and 2.0. We have found that the value of β_{222} is 2.3×10^{-30} esu at zero limit and 6.6×10^{-30} esu at λ = 1.064 μm. The microscopic hyperpolarizability β_{ijk} terms cumulatively yield a bulk observable second-order susceptibility term, $\chi^{(2)}_{ijk}(\omega)$, which in turn is responsible for the high SHG response.[28,29] In Table 4, we present our calculated value of β_{222} in comparison with the experimental data[14] and the available calculated values using different methods.[14] One can see that our calculated value is in better agreement with the measured one than the other theoretical values. This agreement reiterates our faith in the accuracy of the FPLAPW method.

Table 4. Calculated β_{222} in Comparison with the Experimental Data[14] and the Other Calculations[14]

$\beta_{222} \times 10^{-30}$ esu at λ=1.064 μm	
MM3 (molecular mechanics)[a]	3.32
XRC (X-ray analysis)[a]	4.00
AM1 (semiempirical calculation)[a]	3.52
AM1-L (semiempirical calculation)[a]	3.43
AB (ab initio calculations)[a]	3.23
This work	6.60
Exp.[b]	5.04

[a]According to ref 14. [b]ref 14.

dx.doi.org/10.1021/jp3074128 | J. Phys. Chem. B 2012, 116, 13338−13343

4. CONCLUSIONS

The linear, nonlinear optical susceptibilities and hyperpolarizability for $C_{11}H_8N_2O$, *o*-methoxydicyanovinylbenzene, crystals were performed using the FPLAPW method within WIEN2K code. Four different xc potentials were used. There are systematically increased energy gap values from 2.25 eV (LDA), 2.34 eV (GGA), 2.50 eV (EVGGA) to 2.96 eV (mBJ). The titled crystal possesses a direct energy gap and considerable birefringence anisotropy. Further insight into the electronic structure can be obtained from the calculation of the interband optical functions. Furthermore, the nonlinear optical susceptibility dispersions were investigated. We find that the dominant component of the second harmonic generation has a value of about 5.8×10^{-8} esu, which is in good agreement with the measured value 4.9×10^{-8} esu. We also have found that the value of β_{222} (of the dominant component) is 6.6×10^{-30} esu at $\lambda = 1.064$ μm, which is in better agreement with the measured value of 5.04×10^{-30} esu at $\lambda = 1.064$ μm) than the other calculations. Our results suggest that the titled crystal may be promising for NLO effects.

AUTHOR INFORMATION

Corresponding Author

*Tel. +420 777 729 583, Fax. +420-386 361, E-mail maalidph@yahoo.co.uk.

Notes

The authors declare no competing financial interest.

ACKNOWLEDGMENTS

This work was supported from the institutional research concept of the project CENAKVA (no. CZ.1.05/2.1.00/01.0024), the grant no. 152/2010/Z of the Grant Agency of the University of South Bohemia. The School of Materials Engineering, University Malaysia Perlis (UniMAP), Perlis, Malaysia. S.A. thanks Council of Scientific and Industrial Research (CSIR) - National Physical Laboratory for financial support.

REFERENCES

(1) Zyss, J.; Ledoux, I.; Nicoud,J. F. In *Molecular Nonlinear Optics: Materials Physics and Devices*, Zyss, J., Ed.; Academic: Boston, 1994; pp 129−200.

(2) Chelma, D. S.; Zyss, J. In *Nonlinear Optical Properties of Organic Molecules and Crystals*; Academic Press: Orlando, FL, 1987; Vol. *1*.

(3) Marder, S. R.; Sohn, J. E.; Stucky, G. D. In *Materials for Nonlinear Optics: Chemical Perspectives*; ACS Symposium Series 455; American Chemical Society: Washington, DC, 1991.

(4) Lipscomb, G. F.; Garito, A. F.; Narang, R. S. *J. Chem. Phys.* **1981**, *75*, 1509−1516.

(5) Desiraju, G. R. *Acc. Chem. Res.* **2002**, *35*, 565−573. Aakeroy, C. B.; Seddon, K. R. *Chem. Soc. Rev.* **1993**, *22*, 397−407. Saha, B. K.; Nangia, A.; Jaskolski, M. *Cryst. Eng. Comm.* **2005**, *7*, 355−358. Russell, V. A.; Etter, M. C.; Ward, M. D. *J. Am. Chem. Soc.* **1994**, *116*, 1941−1952. Huang, K. S.; Britton, D.; Etter, M. C.; Byrn, S. R. *J. Mater. Chem.* **1995**, *5*, 379−383. Panunto, T. W.; Urbanczyk-Lipkowska, Z.; Johnson, R.; Etter, M. C. *J. Am. Chem. Soc.* **1987**, *109*, 7786−7797.

(6) Custelcean, R. *Chem. Commun. (Cambridge)* **2008**, *3*, 295−307. Yin, Z.; Li, Z. *Tetrahedron Lett.* **2006**, *47*, 7875−7879.

(7) Jazbinsek, M.; Kwon, O. P.; Bosshard, Ch.; Günter, P. In *Handbook of Organic Electronics and Photonics*, Nalwa, S. H., Ed.; American Scientific Publishers: Los Angeles, 2008; Chap. 1; Bosshard, Ch.; Bösch, M.; Liakatas, I.; Jäger, M.; Günter, P. In *Nonlinear Optical Effects and Materials*, Günter, P.,Ed.; Springer-Verlag: Berlin, 2000; Chap. 3; Nalwa, H. S.; Watanabe, T.; Miyata, S. In *Nonlinear Optics of Organic Molecules and Polymers*, Nalwa, H. S., Miyata, S., Eds.; CRC Press: Boca Raton, FL, 1997; Chap. 4.

(8) Zyss, J.; Oudar, J. L. *Phys. Rev. A* **1982**, *26*, 2028−2048.

(9) Kwon, O. P.; Jazbinsek, M.; Seo, J.-I.; Choi, E.-Y.; Yun, H.; Brunner, F. D. J.; Lee, Y. S.; Günter, P. *J. Chem. Phys.* **2009**, *130*, 134708−134714.

(10) Koch, W.; Holthausen, M. C. A. A. *Chemistry Guide to Density Functional Theory*; Wiley-VCH: Weinheim, 2000.

(11) Parr, R. R.; Yang, R. G. *Density Functional Theory of Atoms and Molecules*; Oxford University Press: New York, 1989, and references therein.

(12) Shiwu, G. *Comput. Phys. Commun.* **2003**, *153*, 190−198.

(13) Schwartz, K. *J. Solid State Chem.* **2003**, *176*, 319−328.

(14) Antipin, M; Barr, T; Cardelino, B; Clark, R; Moore, C; Myers, T; Penn, B; Romero, M; Sanghadasa, M; Timofeeva, T. *J. Phys. Chem. B* **1997**, *101*, 2770−2781.

(15) Blaha, P.; Schwarz, K.; Madsen, G. K. H.; Kvasnicka, D.; Luitz, J. *WIEN2K, an Augmented Plane Wave + Local orbitals program for calculating crystal properties*, Schwarz, K., Ed.; Techn. Universitat, Wien, Austria, 2001.

(16) Hohenberg, P.; Kohn, W. *Phys. Rev.* **1964**, *136*, 864−871.

(17) Ceperley, D. M.; Ader, B. I. *Phys. Rev. Lett.* **1980**, *45*, 566−569. parametrized in Perdew, J. P.; Zunger, A. *Phys. Rev. B* **1973**, *8*, 4822−4832.

(18) Perdew, J. P.; Burke, S.; Ernzerhof, M. *Phys. Rev. Lett.* **1996**, *77*, 3865−3868.

(19) Engel, E.; Vosko, S. H. *Phys. Rev. B* **1993**, *47*, 13164−13174.

(20) Tran, F.; Blaha, P. *Phys. Rev. Lett.* **2009**, *102*, 226401−226404.

(21) Tributsch, H. *Z. Naturforsch. A* **1977**, *32A*, 972−985.

(22) Reshak, Ali Hussain; Ph.D. Thesis; Indian Institute of Technology; Rookee, India, 2005.

(23) Sharma, S.; Dewhurst, J. K.; Ambrosch-Draxl, C. *Phys. Rev. B* **2003**, *67*, 165332−165340. Sharma, S.; Ambrosch-Draxl, C. *Physica T* **2004**, *109*, 128−134.

(24) Rashkeev, S. N.; Lambrecht, W. R. L. *Phys. Rev. B* **2001**, *63*, 165212−165223. Rashkeev, S. N.; Lambrecht, W. R. L.; Segall, B. *Phys. Rev. B* **1998**, *57*, 3905−3919.

(25) Saini, H., S.; Singh, M.; Reshak, A. H.; Kashyap, M. K. *J. Alloys Compd.* **2012**, *518*, 74−79.

(26) Reshak, A. H.; Auluck, S. *Physica B* **2007**, *388*, 34−42.

(27) Reshak, A. H.; Auluck, S.; Kityk, I. V. *Appl. Phys. A: Mater. Sci. Process.* **2008**, *91*, 451−457.

(28) Boyd., R. Y. *Principles of Nonlinear Optics*; Academic Press: New York, 1982.

(29) Boyd, R. W. *Nonlinear optics*, 3rd ed.; Academic Press, an imprint of Elsevier, 2008.